The EM structure of the TRAPPIII complex leads to the identification of a requirement for COPII vesicles on the macroautophagy pathway

Dongyan Tan[a,b,1], Yiying Cai[c,1], Juan Wang[d,e], Jinzhong Zhang[d,e], Shekar Menon[d,e,2], Hui-Ting Chou[a,b], Susan Ferro-Novick[d,e,3], Karin M. Reinisch[c,3], and Thomas Walz[a,b,3]

[a]Department of Cell Biology, [b]Howard Hughes Medical Institute, Harvard Medical School, Boston, MA 02115; [c]Department of Cell Biology, Yale University School of Medicine, New Haven, CT 06520; and [d]Department of Cellular and Molecular Medicine, [e]Howard Hughes Medical Institute, University of California, San Diego, La Jolla, CA 92093

Edited by Axel T. Brunger, Stanford University, Stanford, CA, and approved October 22, 2013 (received for review August 29, 2013)

The transport protein particle (TRAPP) III complex, comprising the TRAPPI complex and additional subunit Trs85, is an autophagy-specific guanine nucleotide exchange factor for the Rab GTPase Ypt1 that is recruited to the phagophore assembly site when macroautophagy is induced. We present the single-particle electron microscopy structure of TRAPPIII, which reveals that the dome-shaped Trs85 subunit associates primarily with the Trs20 subunit of TRAPPI. We further demonstrate that TRAPPIII binds the coat protein complex (COP) II coat subunit Sec23. The COPII coat facilitates the budding and targeting of ER-derived vesicles with their acceptor compartment. We provide evidence that COPII-coated vesicles and the ER-Golgi fusion machinery are needed for macroautophagy. Our results imply that TRAPPIII binds to COPII vesicles at the phagophore assembly site and that COPII vesicles may provide one of the membrane sources used in autophagosome formation. These events are conserved in yeast to mammals.

Macroautophagy is a highly conserved catabolic process that uses a specialized membrane trafficking pathway to target proteins and organelles for degradation (1). Defects in this process have been linked to a variety of human diseases, including neurodegenerative diseases such as Parkinson's disease (2). Macroautophagy is induced by a variety of physiological stresses and begins with the expansion of a cup-shaped nucleating membrane called the phagophore, or isolation membrane. As the phagophore expands, it engulfs intracellular proteins and membranes that are marked for degradation. This expanding membrane eventually closes to become an autophagosome, a double-membrane structure that seals its contents from the cytosol and delivers it to the lysosome or vacuole for degradation. A central unanswered question in the autophagy field is the mechanism by which the phagophore forms and matures into an autophagosome. Although it was once thought that the phagophore assembles de novo, recent evidence suggests it forms from a preexisting compartment. Compartments on the secretory pathway, including the endoplasmatic reticulum (ER) and Golgi complex, have been invoked in phagophore assembly (3, 4).

A collection of *ATG* (autophagy-related) genes, the products of which regulate autophagy, were identified in the yeast *Saccharomyces cerevisiae* (1). Many of the Atg proteins needed for macroautophagy in yeast are shared with the biosynthetic cytoplasm to vacuole targeting (Cvt) pathway that transports certain hydrolases into the vacuole. Both pathways require the sequestration of cargo within a double-membrane structure; however, only the macroautophagy pathway is conserved in higher eukaryotes (5). When autophagy is induced, *ATG* gene products assemble at the phagophore assembly site (PAS) in a hierarchical manner. The scaffold protein complex that organizes this site is the Atg17 complex (6, 7).

Previous studies have shown that the transport protein particle (TRAPP) III complex, an autophagy-specic guanine nucleotide exchange factor (GEF) for the Rab GTPase Ypt1, is recruited to the PAS (8) by Atg17 (9). At the PAS, TRAPPIII activates Ypt1 (8), which then recruits its downstream effector, the serine/threonine Atg1 kinase, to the PAS (9). TRAPPIII is one of three multimeric GEFs, called TRAPPI, TRAPPII, and TRAPPIII, that activate Ypt1 on different trafficking pathways (10). TRAPPI, an elongated complex ~18 nm in length (11, 12), binds to ER-derived COPII-coated vesicles via an interaction between the TRAPPI subunit Bet3 and the coat subunit Sec23 (11, 13). The TRAPPIII complex contains the same six subunits present in TRAPPI plus one unique subunit, Trs85, that targets this complex to the PAS (8, 9). Here, we describe the single-particle electron microscopy (EM) structure of TRAPPIII from *S. cerevisiae*. TRAPPIII (23 nm) is longer than TRAPPI with Trs85 capping one end of the complex. As in TRAPPI, the two Bet3 subunits in TRAPPIII are solvent accessible and are available for interaction with Sec23. This observation suggests that TRAPPIII may play a role in tethering COPII-coated vesicles at the PAS. Consistent with this proposal, we find that COPII vesicles accumulate at the PAS when autophagy is blocked. Additionally, we show that mutations in components of the ER-Golgi trafficking machinery, which mediate COPII vesicle fusion, disrupt autophagy. Finally, we find that COPII vesicles accumulate at or near ER-mitochondria contact sites when COS-7 cells are starved. ER-mitochondria contact sites are where autophagosomes form in mammalian cells (14).

Significance

Rab GTPases are critical determinants of membrane identity in eukaryotic cells. Typically, each GTPase is activated by a single guanine nucleotide exchange factor (GEF), but the Ypt1/Rab1 GTPase is activated by three related GEFs, transport protein particle (TRAPP) I, TRAPPII, and TRAPPIII, that function in distinct trafficking pathways. TRAPPIII is recruited to the phagophore assembly site when macroautophagy is induced. Here, we present the single-particle electron microscopy structure of TRAPPIII and evidence that TRAPPIII binds the coat protein complex (COP) II coat. We also show that the ER-Golgi fusion machinery that is present on COPII vesicles is needed for macroautophagy. Our results imply that TRAPPIII recruits COPII vesicles to the PAS and that COPII vesicles may provide one of the membrane sources used in autophagosome formation.

Author contributions: D.T., Y.C., J.W., S.F.-N., K.M.R., and T.W. designed research; D.T., Y.C., J.W., J.Z., S.M., and H.-T.C. performed research; D.T., Y.C., J.W., J.Z., S.M., H.-T.C., S.F.-N., K.M.R., and T.W. analyzed data; and D.T., S.F.-N., K.M.R., and T.W. wrote the paper.

The authors declare no conflict of interest.

This article is a PNAS Direct Submission.

Data deposition: The EM 3D map of TRAPPIII has been deposited in the EMDatabank, http://www.emdatabank.org (accession code EMD-5741).

[1]D.T. and Y.C. contributed equally to this work.

[2]Present address: Affymetric, Inc., Santa Clara, CA 95051.

[3]To whom correspondence may be addressed. E-mail: sfnovick@ucsd.edu, karin.reinisch@yale.edu, or twalz@hms.harvard.edu.

This article contains supporting information online at www.pnas.org/lookup/suppl/doi:10.1073/pnas.1316356110/-/DCSupplemental.

Results and Discussion

EM Structure of the TRAPPIII Complex. To establish the subunit organization of the yeast TRAPPIII complex, we coexpressed the TRAPPIII-specific subunit Trs85 together with all six TRAPPI subunits (Bet3, Bet5, Trs20, Trs23, Trs31, and Trs33) in *Escherichia coli*. The resulting complex was purified by affinity and size exclusion chromatography, and SDS/PAGE analysis showed that all subunits were present (Fig. S1*A*). EM images of the purified recombinant TRAPPIII complex prepared by negative staining showed monodispersed particles that were homogeneous in size and shape (Fig. 1*A*).

To ensure that recombinant TRAPPIII is representative of the native complex, we also purified TRAPPIII from yeast by using a TAP tag on Trs85. SDS/PAGE analysis revealed all TRAPPIII subunits (Fig. S2*A*), which were also identified by mass spectrometry (9). EM images of the complex isolated from yeast showed particles of the same size and overall shape as recombinant TRAPPIII (Fig. S2*B*). To compare the recombinant and native complexes in more detail, we collected 60°/0° tilt pairs of the recombinant complex (Fig. S1*B*) as well as images of the native complex, and calculated projection averages (Figs. S1*C* and S2*C*). The projection average of recombinant TRAPPIII (Fig. 1*B*) shows identical fine structure as that of the native complex (Fig. 1*C*), demonstrating that recombinantly produced TRAPPIII has the same structure as the native complex. Furthermore, comparison of the TRAPPIII average with an average of TRAPPI (Fig. 1*B, Inset*; ref. 12) shows that the lower three-quarters of the TRAPPIII particle is formed by TRAPPI; the top quarter of the particle must therefore represent the TRAPPIII-specific subunit Trs85 (Fig. 1*B*). We proceeded to calculate a 3D map of recombinant TRAPPIII by using the random conical tilt approach (15). The final density map was calculated with 1,120 particles selected from images of the 60°-tilted specimen and 112 particles selected from images of the untilted specimen. The resolution was estimated to be 22 Å according to the Fourier shell correlation (FSC) curve (Fig. S1*D*). Although the side view of the density map adds only limited structural information (Fig. 1*D, Right*), the top view (Fig. 1*D, Left*) shows the same features seen in the projection averages. The banana-shaped TRAPPIII complex has approximate dimensions of 230 Å × 68 Å × 46 Å.

Subunit Organization of the TRAPPIII Complex. The TRAPPI complex can be viewed as an assembly of two subcomplexes (12). In the projection average shown in Fig. 1*B, Inset*, the bottom half with the round end represents the Bet3/Trs33/Bet5/Trs23 subcomplex, whereas the top half with the pointed end represents the Bet3/Trs31/Trs20 subcomplex (12). The extra density in the TRAPPIII projection map representing Trs85 extends from the upper, pointed end of TRAPPI (Fig. 1*B*), suggesting that Trs85 interacts with the Bet3/Trs31/Trs20 subcomplex. Indeed, coexpression of Trs85 in *E. coli* with Bet3, Trs31, and Trs20 yielded a stable complex of all four subunits (Fig. S3*A*), whereas Trs85 is insoluble when coexpressed with the subunits of the other subcomplex, Bet3, Trs33, Bet5, and Trs23, and does not associate with it.

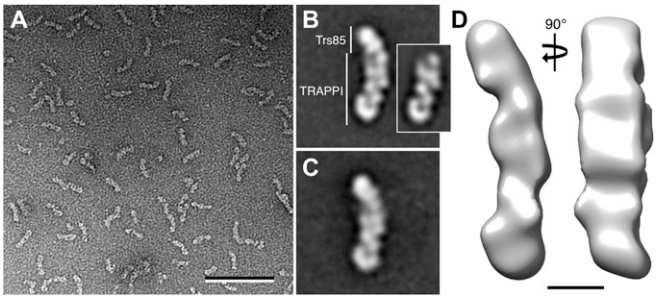

Fig. 1. Single-particle EM analysis of the yeast TRAPPIII complex. (*A*) Representative EM image of negatively stained TRAPPIII complex produced in *E. coli* showing monodispersed, elongated particles. (*B*) A class average of recombinant TRAPPIII revealing a banana-shaped complex ~23 nm in length (see Fig. S1*C* for all class averages). The densities representing TRAPPI and Trs85 are labeled. Side length of image is 36 nm. *Inset* shows a projection average of TRAPPI (12). (*C*) A class average of TRAPPIII purified from *S. cerevisiae* using a TAP tag on Trs85 shows the same structural features as the recombinant complex in *B* (see Fig. S2*C* for all class averages). Side length of image is 36 nm. (*D*) Orthogonal views of the TRAPPIII density map at 22 Å resolution obtained by random conical tilt reconstruction. (Scale bar: *A*, 100 nm; *D*, 5 nm.)

To further verify that Trs85 binds to the Bet3, Trs31, and Trs20 subunits, we purified the Trs85/Bet3/Trs31/Trs20 subcomplex and imaged it by negative stain EM. The EM images showed a homogenous population of particles that appeared to have a similar width as the TRAPPIII full complex but to be shorter (Fig. 2*A*), as confirmed by class averages of the subcomplex (Fig. S3*B*). Closer inspection of the class averages revealed three well-resolved globular densities representing the three TRAPPI subunits, Trs20, Trs31, and Bet3, and an additional dome-shaped density representing Trs85 (Fig. 2*A, Inset*).

Guided by the knowledge that Trs85 binds to the Bet3/Trs31/Trs20 subcomplex, we docked an atomic model of TRAPPI into our EM density map. The TRAPPI model was built by combining the crystal structures of the mammalian Bet3/Trs33/Bet5/Trs23 and Bet3/Trs31/Trs20 subcomplexes (12) based on the crystal structure of the Ypt1-bound TRAPPI core complex (11). The excellent fit of the TRAPPI model into the EM density map of TRAPPIII shows that Trs85 binding does not induce a significant structural reorganization in TRAPPI (Fig. 2*B*). Furthermore, Trs85 binding occupies only a small area on one end of TRAPPI, leaving most of the TRAPPI surface still accessible for interactions with other proteins.

Based on the docking, the major interaction of Trs85 with TRAPPI is mediated by Trs20, in particular helix 1, with a possible contribution of C-terminal helix 5 of Trs31 (Fig. 2*C*). Helix 1 of Trs20 contains residue Asp-46, and mutation of the corresponding aspartate in the mammalian protein (Asp47) to tyrosine causes the human disorder spondyloepiphyseal dysplasia late onset (SEDL) (16, 17). Asp-46 faces straight toward the Trs85 density (Fig. 2*C*), and mutation of this acidic residue to an aromatic residue is thus likely to interfere with Trs85 binding. Indeed, although we are able to prepare the yeast Trs85/Trs20/Bet3/Trs31 subcomplex by coexpressing these proteins in bacteria, we find that under similar conditions, Trs85 does not assemble with Trs20/Bet3/Trs31 and is insoluble when Trs20 bears the SEDL mutation. Consistent with a previous report (18) and our own observation that the D46Y mutation disrupts the interaction of Trs85 with Trs20, we found a defect in the delivery of vacuolar alkaline phosphatase (Pho8Δ60) to the vacuole (Fig. S4). During macroautophagy, Pho8Δ60 is delivered from the cytosol to the vacuole where it is activated (19). Interestingly, Trs20 was also implicated in the interaction of TRAPPI with the TRAPPII-specific subunit Trs130 (20, 21), so the D46Y mutation appears to compromise the formation of both the TRAPPII and TRAPPIII complexes.

Mapping the Binding Site for the Rab GTPase Ypt1 in TRAPPIII. Previous studies have shown that the TRAPP complexes function as GEFs for the Rab GTPase Ypt1 (10). The minimum subcomplex of TRAPPI required for Ypt1 GEF activity contains subunits Bet3, Bet5, Trs23, and Trs31. The crystal structure of this subcomplex with bound Ypt1 revealed that Ypt1 binding is mainly mediated by Trs23 with additional contributions from Bet3 and Bet5 (11). As was reported for TRAPPII, this Ypt1 binding site is freely accessible in TRAPPIII (Fig. 3*A*). To test whether Ypt1 can, as predicted, bind to TRAPPIII, we expressed and purified a GST-Ypt1 fusion protein (Fig. S5*A*), incubated it with TRAPPIII, and collected EM images of negatively stained samples. The raw images show TRAPPIII particles with additional density attached to their sides (Fig. 3*B*), and class averages of TRAPPIII with bound GST-Ypt1 revealed that the extra density representing GST-Ypt1 is located at the expected position (Fig. 3*B, Inset* and Fig. S5*B*),

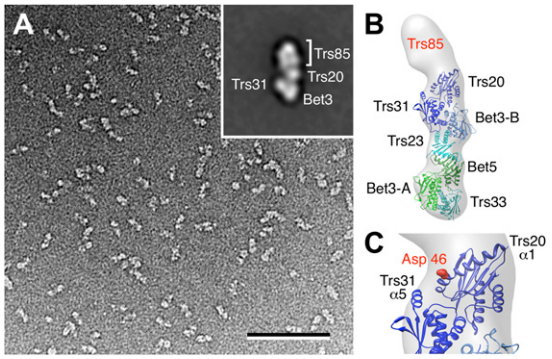

Fig. 2. Subunit organization of the TRAPPIII complex. (*A*) Representative EM image of negatively stained Trs85/Trs20/Trs31/Trs23 subcomplex. (Scale bar: 100 nm.) *Inset* shows a class average of the subcomplex with individual subunits labeled (see Fig. S3*B* for all class averages). Side length of image is 36 nm. (*B*) Atomic model of the TRAPPI complex (generated from three crystal structures; PDB ID codes 2J3T, 2J3W, and 3CUE) fit into the EM density map of TRAPPIII; TRAPPI subunits are labeled in black, and the TRAPPIII-specific Trs85 subunit in red. (*C*) Close-up view of the interface between Trs85 and the Trs20 and Trs31 subunits of TRAPPI. Residue Asp-46 in Trs20 is shown in red; mutation of the corresponding aspartate in the mammalian protein causes SEDL.

indicating that the binding mode of Ypt1 to TRAPPI is conserved in TRAPPIII.

The Trs31 subunit of TRAPPI does not interact with Ypt1 directly, but it is believed to function in the allosteric regulation of the Ypt1-interacting surface (11). Interestingly, the C-terminal helix 5 of Trs31 is positioned at the interface of TRAPPI with Trs85 (Fig. 2*C*) and may thus communicate Trs85 binding to the Ypt1 binding site of TRAPPI. To test whether Trs85 binding affects the GEF activity of the TRAPPI core for Ypt1 in the recombinant complex, we compared the ability of the TRAPPI and TRAPPIII complexes to facilitate GTPγS uptake by Ypt1. As shown in Fig. S5*C*, recombinant TRAPPI and TRAPPIII have comparable GEF activity.

COPII-Coated Vesicles Accumulate at the PAS When Autophagy Is Blocked. The COPII coat is assembled when the activated form of the GTPase Sar1 recruits the inner shell of the coat, the Sec23/Sec24 complex. The coat inner shell then recruits the Sec13/Sec31 complex, which leads to coat polymerization and vesicle budding (22, 23). Previous studies have shown that the TRAPPI complex initiates the tethering of COPII-coated vesicles to their acceptor compartment by binding to the coat subunit Sec23 (13, 24). The coat is then released at the target membrane just before fusion (13).

To address whether the TRAPPIII complex retains its ability to bind to Sec23, we incubated purified recombinant TRAPPIII with GST-Sec23 in vitro. Binding to Sec23 was monitored by following the TRAPP subunit Trs33 (10, 25). As shown in Fig. 3*C*, TRAPPIII bound specifically to GST-Sec23, but not to GST or GST-Sec13, which served as specificity controls. These findings imply that TRAPPIII binds to COPII-coated vesicles. Consistent with this proposal is the recent observation that the mammalian counterpart of Trs85, TRAPPC8, coprecipitates with the COPII coat subunit Sec31A (26).

COPII vesicles bud from a specialized region of the ER, called ER exit sites (ERES). Recently, 3D fluorescence microscopy revealed that the isolation membrane is in close proximity to ERES at several sites within the cell (27, 28). The observation that the autophagy-specific GEF TRAPPIII binds to Sec23 suggested that COPII vesicles may participate in autophagy. To begin to address whether COPII vesicles contribute to macroautophagy, we blocked autophagy in the *atg1*Δ and *atg13*Δ mutants during nitrogen starvation and examined the localization of the ERES by using two different COPII coat subunits, Sec13 and Sec23, fused to GFP. The Atg1 kinase, which is needed for phagophore initiation (29), is a Ypt1 effector that has recently been implicated in membrane tethering events at the PAS (9, 30). Atg13 binds to Atg1 and regulates its kinase activity (31). We also analyzed the localization of Sec13-GFP and Sec23-GFP in the *uso1-1* mutant, because Uso1 is another Ypt1 effector that is known to tether COPII vesicles on a different pathway (ER-Golgi) (32).

In wild-type cells, Sec13-GFP and Sec23-GFP largely reside adjacent to the PAS, which is marked by aminopeptidase I (Ape I). In the *atg1*Δ and *atg13*Δ mutants (Fig. 4 *A–D*), but not in the *uso1-1* mutant (Fig. 4 *E–H*), there was an increase in puncta that colocalized with the PAS and a concomitant decrease in Sec13-GFP and Sec23-GFP puncta adjacent to the PAS. Thus, consistent with the proposal that COPII vesicles are needed for macroautophagy, vesicles begin to accumulate at the PAS in the *atg1*Δ and *atg13*Δ mutants. These findings would explain why the *sec12* mutant, which blocks the budding of COPII vesicles from the ER, is defective in macroautophagy (33, 34). Our findings also suggest that COPII-mediated macroautophagy trafficking events at the PAS may depend on the Ypt1 effector Atg1, but not on Uso1. Thus, distinct Ypt1 effectors may tether COPII vesicles to different acceptor compartments to mediate separate trafficking events.

Components of the ER-Golgi Fusion Machinery Are Needed for Macroautophagy. If COPII vesicles participate in macroautophagy, components of the ER-Golgi fusion machinery that are present on COPII-coated vesicles should also be required for autophagy. COPII vesicles contain the Rab GTPase Ypt1, several soluble N-ethylmaleimide-sensitive factor attachment protein receptor (SNARE) proteins that are needed for membrane fusion (Bet1, Bos1, Sed5, and Sec22) (35, 36), as well as the SNARE-binding protein Sly1 (37). To address whether these secretory components are needed for macroautophagy, we starved the *sec12-4*, *bos1-1, bet1-1, sed5-1*, and *sly1*^{ts} temperature-sensitive (ts) mutants and their isogenic wild-type strains for nitrogen at 37 °C for 2 h. To determine whether these ts mutants disrupt autophagy, we quantitatively measured autophagic activity by using the Pho8Δ60 assay. When yeast cells are starved for nitrogen, the secretory pathway is downregulated (38) and, as a consequence, the secretory defect in these ts mutants is dramatically reduced or not apparent (Fig. S6). A defect in macroautophagy was observed in the *bos1-1*, *bet1-1, sed5-1*, and *sly1*^{ts} mutants (Fig. 5), as well as the *sec12-4* mutant, which served as a control (33). The fourth SNARE that acts in ER-Golgi traffic, Sec22, was previously shown to be required for macroautophagy in both yeast and mammalian cells (14, 39). In contrast, the *uso1-1* mutant was not defective in macroautophagy (Fig. 5). These results imply that the ER-Golgi fusion machinery, but not the tether Uso1, are needed for macroautophagy. Together, our

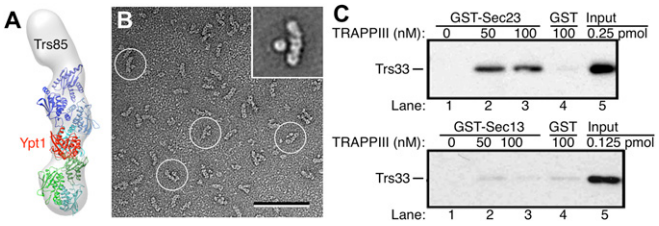

Fig. 3. Mapping the binding site for Ypt1 in TRAPPIII. (*A*) Atomic model of Ypt1 bound to TRAPPI (generated from three crystal structures; PDB ID codes 2J3T, 2J3W, and 3CUE) was fit into the EM density map of TRAPPIII. (*B*) Representative EM image of negatively stained TRAPPIII incubated with a GST-Ypt1 fusion protein. Circles indicate TRAPPIII particles with bound GST-Ypt1. (Scale bar: 100 nm.) *Inset* shows a class average of TRAPPIII with bound GST-Ypt1 (see Fig. S5*B* for all class averages). Side length of *Inset* is 36 nm. (*C*) Recombinant TRAPPIII binds to Sec23, but not to Sec13. Purified TRAPPIII was incubated for 3 h at 4 °C with equimolar amounts (100 nM) of immobilized GST, GST-Sec23, or GST-Sec13. The beads were pelleted, washed, and bound protein was eluted and analyzed by Western blot analysis.

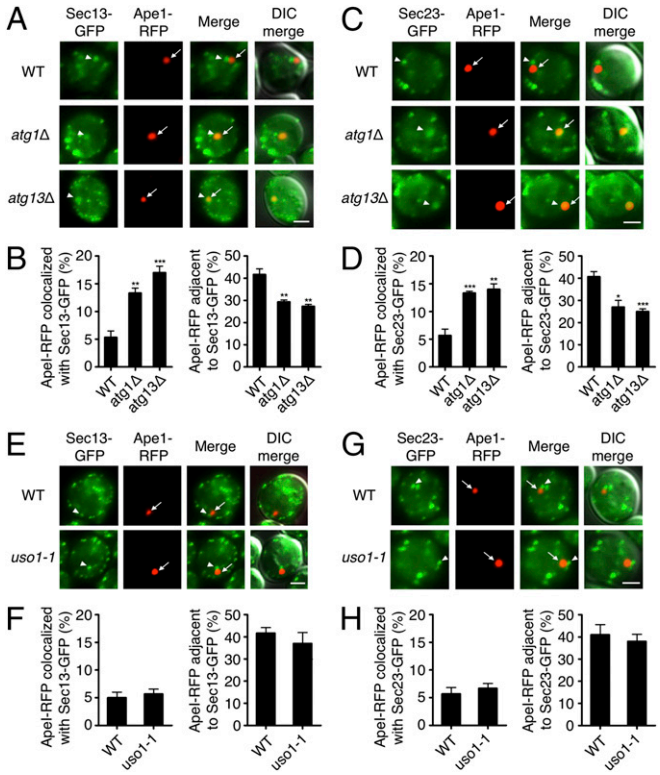

Fig. 4. Sec13 and Sec23 accumulate at the PAS when autophagy is blocked. (*A*) Log phase wild-type (WT), *atg1*Δ, and *atg13*Δ cells expressing Sec13-GFP and Ape1-RFP were pelleted, resuspended in SD-N medium, and incubated at 25 °C for 4 h before they were examined by fluorescence microscopy. Arrowheads point to Sec13-GFP puncta, and arrows point to Ape1-RFP. (*B*) One hundred fifty cells from three separate experiments were examined to calculate the percentage of Ape I-RFP puncta that colocalize with (*Left*) or lie adjacent to (*Right*) Sec13-GFP puncta. Error bars represent SEM. $^{**}P < 0.01$, $^{***}P < 0.001$ Student's *t* test. (*C*) WT, *atg1*Δ, and *atg13*Δ cells expressing Sec23-GFP and Ape1-RFP were treated as in *A*. Arrowheads point to Sec23-GFP puncta, and arrows point to Ape1-RFP. (*D*) One hundred fifty cells from three separate experiments were examined to calculate the percent of Ape I-RFP puncta that colocalize with (*Left*) or lie adjacent to (*Right*) Sec23-GFP puncta. Error bars represent SEM. $^{*}P < 0.05$, $^{**}P < 0.01$, $^{***}P < 0.001$ Student's *t* test. (*E*) Log-phase WT and *uso1-1* cells expressing Sec13-GFP and Ape1-RFP were resuspended in SD-N medium and incubated at 37 °C for 2 h before they were examined by fluorescence microscopy. Arrowheads point to Sec13-GFP puncta, and arrows point to Ape1-RFP. (*F*) One hundred fifty cells from three separate experiments were examined to calculate the percent of Ape I-RFP puncta that colocalize with (*Left*) or lie adjacent to (*Right*) Sec13-GFP puncta. Error bars represent SEM. (*G*) WT and *uso1-1* cells expressing Sec23-GFP and Ape1-RFP were treated the same as cells in *E*. Arrowheads point to Sec23-GFP puncta, and arrows point to Ape1-RFP. (*H*) One hundred fifty cells from three separate experiments were examined to calculate the percent of Ape I-RFP puncta that colocalize with (*Left*) or lie adjacent to (*Right*) Sec23-GFP puncta. Error bars represent SEM. (Scale bars: 2 μm.)

findings indicate that when yeast cells are starved for nitrogen, COPII vesicles are diverted from the secretory pathway to the macroautophagy pathway. These findings are consistent with two recent reports in the literature. One report links ER exit sites to autophagosome formation (28), whereas the other study links a compartment formed from COPII and COPI vesicles in mammals (ER-Golgi intermediate compartment; ERGIC) to autophagosome biogenesis (40).

COPII Vesicles Localize to the ER-Mitochondria Contact Sites in Starved COS-7 Cells. It has been reported that autophagosome formation is initiated at ER-mitochondria contact sites in mammalian cells (14). An expectation of the findings we report here is that COPII vesicles should accumulate at these sites. To address this possibility, we examined the localization of the COPII coat subunit Sec31A in starved COS-7 cells. For our studies, the ER network was marked by GFP-Sec61β and the mitochondria by TOMM20. In starved cells, almost half the Sec31A puncta were found adjacent to the ER-mitochondria contact sites or on both ER and mitochondria (Fig. S7 and Table 1), whereas the remaining puncta were only on the ER (Table 1). The localization of a significant fraction of the Sec31A puncta at or near the ER-mitochondria contact sites is consistent with the proposal that COPII vesicles are a membrane source for autophagosomal membranes at these contact sites.

Concluding Remarks. In conclusion, the single-particle EM structure of the TRAPPIII complex shows that the Bet3 subunit of this TRAPP complex should retain its ability to bind to the COPII coat. We present several lines of evidence that support the proposal that TRAPPIII participates in COPII vesicle tethering at the PAS. First, the TRAPPIII complex binds directly to the COPII coat subunit Sec23 in vitro. Second, our findings suggest that COPII-coated vesicles accumulate at the PAS in yeast when autophagy is blocked. Additionally, ts mutants in components of the ER-Golgi fusion machinery, present on the vesicles, are defective in macroautophagy.

When macroautophagy is induced, 30- to 60-nm motile vesicles containing the transmembrane protein Atg9 are sorted at the trans-Golgi network and traffic to the PAS where they tether and fuse to each other or to membranes derived from other compartments, such as the ER (4). We recently suggested that Ypt1 regulates membrane-tethering events at the PAS via its effector Atg1 (9). The findings we report here raise the intriguing possibility that COPII vesicles are one of the partners in Atg1-mediated membrane tethering. We envision the following sequence of events (Fig. 6): TRAPPIII binds to a COPII vesicle via an interaction with Sec23 before it recruits and activates Ypt1. This then leads to the binding of Atg1 to the vesicle, followed by the tethering of the COPII vesicle to an Atg9 vesicle. A more definitive description of the tethering reaction that TRAPPIII and Ypt1 regulate will require the development of a COPII-dependent

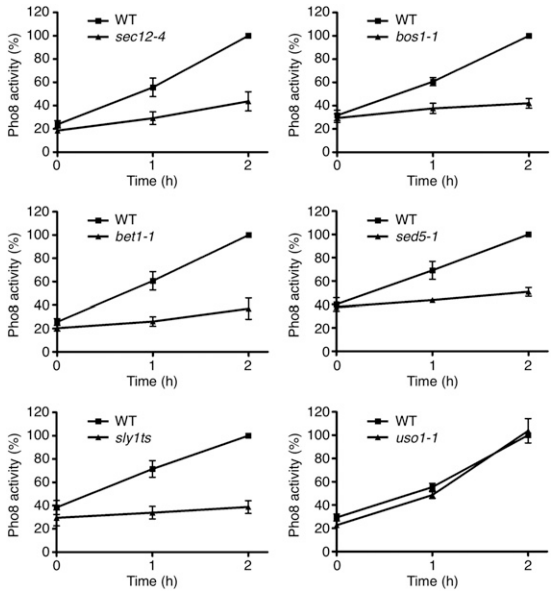

Fig. 5. Macroautophagy is blocked in the *sec12-4*, *bos1-1*, *bet1-1*, *sed5-1*, and *sly1*^{ts} mutants, but not in the *uso1-1* mutant. Cells were grown to log phase in YPD medium at 25 °C, shifted to SD-N medium at 37 °C for 0, 1, and 2 h, and lysed with glass beads. An equal amount of protein was assayed for vacuolar alkaline phosphatase activity. Protein concentration was measured by using the Bradford assay.

Table 1. Quantification of Sec31A localization (n = 1,396)

Localization of Sec31A puncta	Number	Percentage
Adjacent to or on both ER and mitochondria	649	46.5
On ER only	744	53.3
Adjacent to or on mitochondria only	0	0.0
On neither organelle	3	0.2

in vitro tethering assay by using Atg9 vesicles as the acceptor compartment.

Materials and Methods

Cloning for TRAPPIII Complexes. Coding sequences for *BET3*, *BET5*, *TRS20*, *TRS23*, *TRS31*, *TRS33*, and *TRS85* from *S. cerevisiae* were PCR amplified from yeast genomic DNA and cloned into Duet vectors (Novagen). Specifically, *BET3* and *TRS33* were cloned into pETDuet-1, *TRS85* into pCOLADuet-1, *TRS31* and *TRS20* into pCDFDuet-1, and *BET5* and *TRS23* into pACYCDuet-1 vector. A second pETDuet-1 plasmid was constructed containing only the gene for *BET3*. For purification purposes, Trs85 has an N-terminal hexahistidine-SUMO tag, which can be removed by cleavage with SUMO protease.

The recombinant TRAPPI complex (for GEF assays) was expressed and purified as described (11).

Overexpression and Purification of Recombinant TRAPPIII Complexes. For the overexpression of the Trs85/Trs20/Bet3/Trs31 subcomplex of TRAPPIII, the three Duet plasmids harboring genes for *BET3*, *TRS20* and *TRS31*, and *TRS85* were cotransformed into *E. coli* BL21(DE3) cells by electroporation. For the intact complex, the four Duet plasmids harboring genes for all TRAPPIII components were cotransformed into *E. coli* BL21(DE3). The cells were grown at 37 °C to an OD_{600} of ∼0.6–0.8, then were shifted to 20 °C before induction with 0.5 mM IPTG. Cells were harvested 18 h after induction. Both intact TRAPPIII and the Trs85/Trs20/Bet3/Trs31 subcomplex were purified by Ni-NTA chromatography (Qiagen). Complexes were treated with SUMO protease to remove tags from Trs85, then further purified by gel filtration on a Superdex200 column (GE Healthcare). The gel filtration buffer contained 20 mM Hepes at pH 8.0, 300 mM NaCl, and 0.5 mM TCEP.

Purification of Native TRAPPIII. To purify the native TRAPPIII complex, a yeast strain was used with a tandem affinity purification (TAP) tag on the TRAPPIII-specific subunit Trs85 (8). Cells were grown at 30 °C in YPD medium, harvested at OD = 2, frozen, and lysed with a Retsch MM400 mixer mill. TRAPPIII was purified by using the conventional TAP protocol (41). The final elution fraction was used to prepare negatively stained samples for EM. For SDS/PAGE analysis, the complex was precipitated with trichloroacetic acid.

Formation of the TRAPPIII–Ypt1 Complex. The GST-Ypt1 fusion protein was expressed and purified as described (20). Because no GTP was supplemented during the final gel filtration step, purified Ypt1 will be mostly in the GDP-bound form.

To form a complex of TRAPPIII with Ypt1, GST-Ypt1 (∼35 μg) was mixed with TRAPPIII at a molar ratio of 5:1 in 50 mM Tris·HCl at pH 8.0, 150 mM NaCl, 1 mM EDTA, and 1 mM DTT. Negatively stained samples were prepared after a 2-h incubation at room temperature.

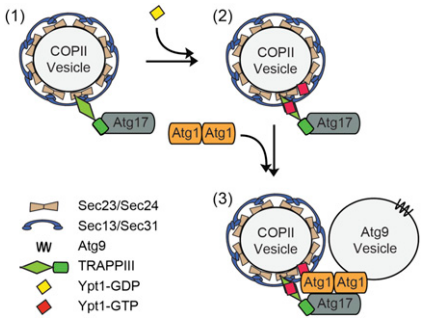

Fig. 6. A model for the early steps of phagophore formation (1). Atg17 recruits TRAPPIII to the PAS, where it binds to a COPII coated vesicle via an interaction with Sec23 (2). TRAPPIII activates Ypt1, and activated Ypt1 recruits its effector, Atg1, to tether a COPII vesicle to an Atg9 vesicle (3).

Nucleotide Exchange Assays. GTPγS uptake activity was monitored and measured as described (42). Briefly, the TRAPPI or TRAPPIII complexes (163 nM) and Ypt1 (114 nM) were incubated in assay buffer (50 mM Tris at pH 8.0, 5 mM $MgCl_2$, 1 mM EDTA, 1 mM DTT, and 1 mg/mL BSA) at room temperature. Exchange reactions were initiated by the addition of 10 μL of ^{35}S-GTPγS (Perkin-Elmer; 1,250 Ci/mmol, diluted to 12.5 μCi/mmol) in a 70-μL reaction mixture. To stop the reaction, samples (10 μL) were removed at 0, 5, 10, 15, and 20 min and added to 1 mL of ice-cold stop buffer (20 mM Tris at pH 8.0 and 250 mM $MgCl_2$) on ice. The samples were then loaded on nirocelllulose filters and washed three times with 3 mL of stop buffer. The filters were dried and counted in a scintillation counter.

In Vitro Binding Experiments. Different concentrations of purified TRAPPIII were incubated for 3 h at 4 °C with equimolar amounts (100 nM) of GST or GST fusion proteins in binding buffer [50 mM Hepes at pH 7.2, 150 mM NaCl, 1 mM EDTA, 1 mM DTT, 0.5 mM $MgCl_2$, 2% (vol/vol) Triton X-100, and 1× protease inhibitor cocktail]. The beads were washed and eluted in SDS/PAGE sample buffer. Bound protein was fractionated on a 13% (wt/vol) SDS polyacrylamide gel and immunoblotted with anti-Trs33 antibody. The concentration of purified TRAPPIII was calculated based on the concentration of Trs33 on a Coomassie blue-stained 13% (wt/vol) SDS polyacrylamide gel by using BSA as a standard.

Media and Growth Conditions for in Vivo Yeast Experiments. Cells were grown at 25 °C in SMD [synthetic minimal medium containing 0.67% yeast nitrogen base, 2% (wt/vol) glucose, and essential amino acids] medium. To induce nitrogen starvation, SD-N [0.17% yeast nitrogen base without amino acids and ammonium sulfate, and 2% (wt/vol) glucose] medium was used.

Fluorescence Microscopy with Yeast. Yeast cells were cultured in SMD selective medium at 25 °C to log phase. To induce autophagy by nitrogen starvation, cells were washed twice and shifted to SD-N medium at 25 °C for 4 h. To induce autophagy in ts mutants and their isogenic wild type, cells were washed twice and shifted to SD-N medium at 37 °C for 2 h. Fluorescent cells were visualized on an Axio Imager Z1 fluorescence microscope by using a 100× oil-immersion objective. Images were captured with an AxioCam MRm digital camera and AxioVision software.

Mammalian Cell Culture and Fluorescence. COS-7 cells were grown at 37 °C in DMEM (Life Technologies) supplemented with 10% (vol/vol) FBS (Life Technologies) and transfected with GFP-Sec61β by using Lipofectamine 2000 (Life Technologies) according to the manufacturer's instructions. Approximately 48 h after transfection, the cells were starved as described (43). The starved cells were washed three times with PBS, fixed with 4% (vol/vol) formaldehyde at room temperature for 15 min, and permeabilized with 0.1% Triton X-100 at room temperature for 5 min. The cells were washed with PBS and incubated with PBS plus 10% (wt/vol) BSA for 60 min without antibody. The cells were incubated for 1 h with anti-TOMM20 (Abcam) and anti-Sec31A (BD Biosciences) antibodies, and washed three times with PBS. The cells were then incubated with Alexa 405 and Alexa 594 (Life Technologies) in the same buffer for another 1 h, and washed three times with PBS. The coverslips were mounted on a glass slide with Fluoremount-G (Southern Biotech). Images were taken with an Olympus IX81 inverted confocal microscope by using a 100× objective. The Sec31A puncta were quantified as described (14).

Pho8Δ60 Assay. Alkaline phosphatase assays were performed as described (19) by using a cytosolic form of Pho8 (Pho8Δ60). Cells were cultured overnight in SMD selective medium at 25 °C to log phase. To induce autophagy by nitrogen starvation, the cells were washed twice and shifted to SD-N medium, and lysed with ice-cold lysis buffer (20 mM Pipes at pH 7.2, 0.5% Triton X-100, 50 mM KCl, 100 mM potassium acetate, 10 mM $MgSO_4$, 10 μM ZnSO4, and 1 mM PMSF) by using glass beads. Samples were assayed at 37 °C with assay buffer (1.25 mM p-nitrophenyl phosphate, 250 mM Tris·HCl at pH 8.5, 0.4% Triton X-100, 10 mM $MgSO_4$, and 10 μM ZnSO4), and reactions were stopped with stop buffer (1 M glycine/KOH at pH 11.0). The OD_{400} value was measured by using an Ultrospec 3100 pro UV/Visible spectrophotometer. The Bradford method was used to measure protein concentration.

Electron Microscopy. Purified proteins were negatively stained with 0.75% uranyl formate solution as described (44). Samples were inspected with

a CM10 electron microscope (Philips) operated at an acceleration voltage of 100 kV, and images were collected with a 2K × 2K CCD camera (Gatan) at a nominal magnification of 52,000×.

Images for further processing were collected with a Tecnai T12 electron microscope (FEI) operated at an acceleration voltage of 120 kV. Images were recorded on imaging plates at a nominal magnification of 67,000× and a defocus of approximately −1.5 μm by using low-dose procedures. Imaging plates were read out with a scanner (DITABIS) by using a step size of 15 μm, a gain setting of 20,000, and a laser power setting of 30% (45). The images were binned over 2 × 2 pixels, yielding a pixel size of 4.5 Å at the specimen level. For 3D reconstruction, the same specimen areas were imaged twice, first at a tilt angle of 60° and then at 0°.

Image Processing. For recombinant TRAPPIII expressed in *E. coli*, 133 60°/0° image pairs were collected, and 9,862 particle pairs were interactively selected by using WEB, the display program of the SPIDER software package (46). The particles were then windowed into 80 × 80-pixel images, which were normalized, rotationally and translationally aligned, and subjected to 10 cycles of multireference alignment. Each round of multireference alignment was followed by K-means classification specifying 20 output classes. The references used for the first multireference alignment were randomly chosen from the particle images. Twelve of the 20 class averages looked similar and showed fine structure, and the particles of these classes were combined (4,956 particles). A 3D reconstruction was then calculated with the particle images from the tilted specimen by using the backprojection and backprojection refinement procedures in SPIDER. The resolution of this density map was 30 Å according to the FSC = 0.5 criterion (47). A second 3D map was calculated by using only the two most similar classes (marked by asterisks in Fig. S1*C*). This density map included 1,120 particles selected from images of the 60°-tilted specimen and 112 particles from images of the untilted specimen. The resolution of this map was estimated as 22 Å (Fig. S1*D*), and the map was filtered to this resolution (Fig. 1*D*). The improvement in resolution using a smaller number of particles suggests that the differences seen in the class averages represent slightly different conformations of TRAPPIII rather than different orientations. The 3D map has been deposited in the EMDatabank (accession code EMD-5741).

For native TRAPPIII purified from *S. cerevisiae*, 7,105 particles were selected from 55 images by using BOXER, the display program of the EMAN software package (48). For the Trs85/Trs20/Trs31/Trs23 subcomplex, 6,657 particles were selected from 76 images, and for TRAPPIII in complex with GST-Ypt1, 1,956 particles were selected from 112 images. Particles for these datasets were windowed into 80 × 80-pixel images and classified into 20 classes as described above.

ACKNOWLEDGMENTS. We thank Shuliang Chen for advice, Wenyun Zhou for technical assistance, and Ben Glick for the Sec13-GFP and Sec23-GFP constructs. We also thank the University of California, San Diego Neuroscience Microscopy shared facility funded by Grant P30 NS047101. Y.C. and K.M.R. were supported by National Institutes of Health (NIH) Grant GM080616. Work at Harvard Medical School was also supported by NIH Grant P01 GM0622580 (to Stephen C. Harrison). Salary support for D.T., J.W., J.Z., S.M., H.-T.C., S.F.-N., and T.W. was provided by the Howard Hughes Medical Institute.

1. Nakatogawa H, Suzuki K, Kamada Y, Ohsumi Y (2009) Dynamics and diversity in autophagy mechanisms: Lessons from yeast. *Nat Rev Mol Cell Biol* 10(7):458–467.
2. Mizushima N, Levine B, Cuervo AM, Klionsky DJ (2008) Autophagy fights disease through cellular self-digestion. *Nature* 451(7182):1069–1075.
3. Tooze SA, Yoshimori T (2010) The origin of the autophagosomal membrane. *Nat Cell Biol* 12(9):831–835.
4. Yamamoto H, et al. (2012) Atg9 vesicles are an important membrane source during early steps of autophagosome formation. *J Cell Biol* 198(2):219–233.
5. Meijer WH, van der Klei IJ, Veenhuis M, Kiel JA (2007) ATG genes involved in non-selective autophagy are conserved from yeast to man, but the selective Cvt and pexophagy pathways also require organism-specific genes. *Autophagy* 3(2):106–116.
6. Kabeya Y, et al. (2009) Characterization of the Atg17-Atg29-Atg31 complex specifically required for starvation-induced autophagy in Saccharomyces cerevisiae. *Biochem Biophys Res Commun* 389(4):612–615.
7. Suzuki K, Kubota Y, Sekito T, Ohsumi Y (2007) Hierarchy of Atg proteins in pre-autophagosomal structure organization. *Genes Cells* 12(2):209–218.
8. Lynch-Day MA, et al. (2010) Trs85 directs a Ypt1 GEF, TRAPPIII, to the phagophore to promote autophagy. *Proc Natl Acad Sci USA* 107(17):7811–7816.
9. Wang J, et al. (2013) Ypt1 recruits the Atg1 kinase to the preautophagosomal structure. *Proc Natl Acad Sci USA* 110(24):9800–9805.
10. Barrowman J, Bhandari D, Reinisch K, Ferro-Novick S (2010) TRAPP complexes in membrane traffic: Convergence through a common Rab. *Nat Rev Mol Cell Biol* 11(11):759–763.
11. Cai Y, et al. (2008) The structural basis for activation of the Rab Ypt1p by the TRAPP membrane-tethering complexes. *Cell* 133(7):1202–1213.
12. Kim YG, et al. (2006) The architecture of the multisubunit TRAPP I complex suggests a model for vesicle tethering. *Cell* 127(4):817–830.
13. Lord C, et al. (2011) Sequential interactions with Sec23 control the direction of vesicle traffic. *Nature* 473(7346):181–186.
14. Hamasaki M, et al. (2013) Autophagosomes form at ER-mitochondria contact sites. *Nature* 495(7441):389–393.
15. Radermacher M (1988) Three-dimensional reconstruction of single particles from random and nonrandom tilt series. *J Electron Microsc Tech* 9(4):359–394.
16. Gedeon AK, et al. (1999) Identification of the gene (SEDL) causing X-linked spondyloepiphyseal dysplasia tarda. *Nat Genet* 22(4):400–404.
17. Gedeon AK, et al. (2001) The molecular basis of X-linked spondyloepiphyseal dysplasia tarda. *Am J Hum Genet* 68(6):1386–1397.
18. Zong M, et al. (2011) The adaptor function of TRAPPC2 in mammalian TRAPPs explains TRAPPC2-associated SEDT and TRAPPC9-associated congenital intellectual disability. *PLoS ONE* 6(8):e23350.
19. Klionsky DJ (2007) Monitoring autophagy in yeast: The Pho8Delta60 assay. *Methods Mol Biol* 390:363–371.
20. Yip CK, Berscheminski J, Walz T (2010) Molecular architecture of the TRAPPII complex and implications for vesicle tethering. *Nat Struct Mol Biol* 17(11):1298–1304.
21. Taussig D, Lipatova Z, Kim JJ, Zhang X, Segev N (2013) Trs20 is required for TRAPP II assembly. *Traffic* 14(6):678–690.
22. Lee MC, Miller EA, Goldberg J, Orci L, Schekman R (2004) Bi-directional protein transport between the ER and Golgi. *Annu Rev Cell Dev Biol* 20:87–123.
23. Zanetti G, Pahuja KB, Studer S, Shim S, Schekman R (2012) COPII and the regulation of protein sorting in mammals. *Nat Cell Biol* 14(1):20–28.
24. Cai H, et al. (2007) TRAPPI tethers COPII vesicles by binding the coat subunit Sec23. *Nature* 445(7130):941–944.
25. Sacher M, et al. (2001) TRAPP I implicated in the specificity of tethering in ER-to-Golgi transport. *Mol Cell* 7(2):433–442.
26. Bassik MC, et al. (2013) A systematic mammalian genetic interaction map reveals pathways underlying ricin susceptibility. *Cell* 152(4):909–922.
27. Suzuki K, Akioka M, Kondo-Kakuta C, Yamamoto H, Ohsumi Y (2013) Fine mapping of autophagy-related proteins during autophagosome formation in Saccharomyces cerevisiae. *J Cell Sci* 126(Pt 11):2534–2544.
28. Graef M, Friedman JR, Graham C, Babu M, Nunnari J (2013) ER exit sites are physical and functional core autophagosome biogenesis components. *Mol Biol Cell* 24(18):2918–2931.
29. Kawamata T, Kamada Y, Kabeya Y, Sekito T, Ohsumi Y (2008) Organization of the pre-autophagosomal structure responsible for autophagosome formation. *Mol Biol Cell* 19(5):2039–2050.
30. Ragusa MJ, Stanley RE, Hurley JH (2012) Architecture of the Atg17 complex as a scaffold for autophagosome biogenesis. *Cell* 151(7):1501–1512.
31. Kamada Y, et al. (2000) Tor-mediated induction of autophagy via an Apg1 protein kinase complex. *J Cell Biol* 150(6):1507–1513.
32. Cao X, Ballew N, Barlowe C (1998) Initial docking of ER-derived vesicles requires Uso1p and Ypt1p but is independent of SNARE proteins. *EMBO J* 17(8):2156–2165.
33. Ishihara N, et al. (2001) Autophagosome requires specific early Sec proteins for its formation and NSF/SNARE for vacuolar fusion. *Mol Biol Cell* 12(11):3690–3702.
34. Novick P, Field C, Schekman R (1980) Identification of 23 complementation groups required for post-translational events in the yeast secretory pathway. *Cell* 21(1):205–215.
35. Lian JP, Ferro-Novick S (1993) Bos1p, an integral membrane protein of the endoplasmic reticulum to Golgi transport vesicles, is required for their fusion competence. *Cell* 73(4):735–745.
36. Barlowe C, et al. (1994) COPII: A membrane coat formed by Sec proteins that drive vesicle budding from the endoplasmic reticulum. *Cell* 77(6):895–907.
37. Cao X, Barlowe C (2000) Asymmetric requirements for a Rab GTPase and SNARE proteins in fusion of COPII vesicles with acceptor membranes. *J Cell Biol* 149(1):55–66.
38. Geng J, Nair U, Yasumura-Yorimitsu K, Klionsky DJ (2010) Post-Golgi Sec proteins are required for autophagy in Saccharomyces cerevisiae. *Mol Biol Cell* 21(13):2257–2269.
39. Nair U, et al. (2011) SNARE proteins are required for macroautophagy. *Cell* 146(2):290–302.
40. Ge L, Melville D, Zhang M, Schekman R (2013) The ER-Golgi intermediate compartment is a key membrane source for the LC3 lipidation step of autophagosome biogenesis. *Elife* 2:e00947.
41. Puig O, et al. (2001) The tandem affinity purification (TAP) method: A general procedure of protein complex purification. *Methods* 24(3):218–229.
42. Wang W, Sacher M, Ferro-Novick S (2000) TRAPP stimulates guanine nucleotide exchange on Ypt1p. *J Cell Biol* 151(2):289–296.
43. Hailey DW, et al. (2010) Mitochondria supply membranes for autophagosome biogenesis during starvation. *Cell* 141(4):656–667.
44. Ohi M, Li Y, Cheng Y, Walz T (2004) Negative staining and image classification – powerful tools in modern electron microscopy. *Biol Proced Online* 6:23–34.
45. Li Z, Hite RK, Cheng Y, Walz T (2010) Evaluation of imaging plates as recording medium for images of negatively stained single particles and electron diffraction patterns of two-dimensional crystals. *J Electron Microsc (Tokyo)* 59(1):53–63.
46. Frank J, et al. (1996) SPIDER and WEB: Processing and visualization of images in 3D electron microscopy and related fields. *J Struct Biol* 116(1):190–199.
47. Böttcher B, Wynne SA, Crowther RA (1997) Determination of the fold of the core protein of hepatitis B virus by electron cryomicroscopy. *Nature* 386(6620):88–91.
48. Ludtke SJ, Baldwin PR, Chiu W (1999) EMAN: Semiautomated software for high-resolution single-particle reconstructions. *J Struct Biol* 128(1):82–97.